Electromagnetically induced transparency in the strong blockade regime using the four-photon excitation process in thermal rubidium vapor

Tanim Firdoshi ●,* Sujit Garain, Vishu Gupta, Dushmanta Kara, and Ashok K. Mohapatra ●†

National Institute of Science Education and Research Bhubaneswar, HBNI, Jatni 752050, India

We present a theoretical model of a four-photon excitation process to the Rydberg state in thermal atomic vapor where the motion-induced dephasing in the system is eliminated. This is achieved by arranging the four laser beams in a suitable geometry such that the residual wave vector is reduced to zero. The method of adiabatic elimination has been used to reduce the complex five-level system to an effective three-level system to study electromagnetically induced transparency (EIT) where the transition from ground state to second excited state can be considered as the effective probe and second excited state to the Rydberg state as the effective coupling transition. The effect of the blockade phenomenon is observed in the strong interaction regime, where the two atoms are considered to be moving with independent velocities and the system is Doppler averaged using Monte Carlo simulation technique. Also, the dephasing mechanisms in the system are investigated in detail. Though the system is not frozen during the excitation process, a strong blockade effect is still observed similar to the cold atom system. We conclude the paper with a proposal for experimentally investigating the four-photon excitation process to the Rydberg state in thermal rubidium vapor.

I. INTRODUCTION

In the last decade, Rydberg atoms [1] have emerged as a promising tool for studying quantum many-body systems with great applications, such as the development of quantum simulators [2], nonequilibrium quantum engines [3], etc. Rydberg atoms are also used to study induced enhanced optical nonlinearity at the level of a single photon [4], sensing radiation ranging from radio frequency to THz [5–8]. Strong interaction in the Rydberg state [9] leading to the phenomenon of Rydberg blockade [10] is at the heart of study of quantum many-body physics. The combination of strong Rydberg-Rydberg interaction with coherent atom-light interaction in electromagnetically induced transparency (EIT) [11,12] possesses enhanced optical nonlinearity [13–15] and has been used to study strong nonlinearity at the level of a single photon [16–19]. The Rydberg blockade requires the system to be frozen during the excitation process and hence, ultracold atoms are only used for such experiments [20–24]. Recently, there have been experiments to study Rydberg interaction and blockade-induced effects in thermal vapor [25] using nanosecond pulses [26]. Again, the thermal vapor system is frozen in a nanosecond timescale, which makes such experiments feasible.

In this paper, we propose a four-photon excitation process to study EIT in the strong blockade regime where the system is not necessarily be frozen during the excitation process. Such experiments can be done using cw lights and the system can be studied in the steady state. To study the Rydberg excitation in thermal atomic vapor, multiphoton excitation schemes have been used in various experiments [27–31], where the diode lasers are inexpensive and also higher Rabi frequencies can be achieved using low laser power. The main idea of the proposal is to use a suitable geometry of the four laser beams such that the residual wave vector of the lasers is nearly zero, hence eliminating the motion-induced dephasing in the system. Motion-induced dephasing is a serious issue for experiments involving Rydberg interactions. There are studies [32,33] and a proposal [34] on how to eliminate the motional dephasing in the atomic system, but the four-photon Rydberg excitation scheme has not been discussed and analyzed in detail. Such experiments with thermal vapor are simpler compared to the complexity involved in the cold atomic system. Hence, it will be useful for practical applications of building quantum devices as the Rydberg atomic systems have been evolving to be the basis of various quantum technologies [35].

The paper is organized as follows. In the next section, we discuss a model of the five-level system to study EIT using the four-photon excitation process to the Rydberg state. In Sec. III, the method of adiabatic elimination [36] is shown where we reduce the complex five-level system to an effective three-level system followed by the study of EIT in the strong blockade regime using a model with two interacting atoms in the Rydberg states in Sec. IV. Finally, in Sec. V, we give an experimental proposal with thermal rubidium vapor.

II. FOUR-PHOTON EXCITATION IN A FIVE-LEVEL SYSTEM

Let us consider a five-level atomic system with states $|g\rangle$, $|e\rangle$, $|e'\rangle$, $|e''\rangle$, and $|r\rangle$ in a ladder configuration as shown in Fig. 1(a), where $|g\rangle$ is the ground state, $|r\rangle$ is the Rydberg state,

---

*tanim.firdoshi@niser.ac.in
†a.mohapatra@niser.ac.in
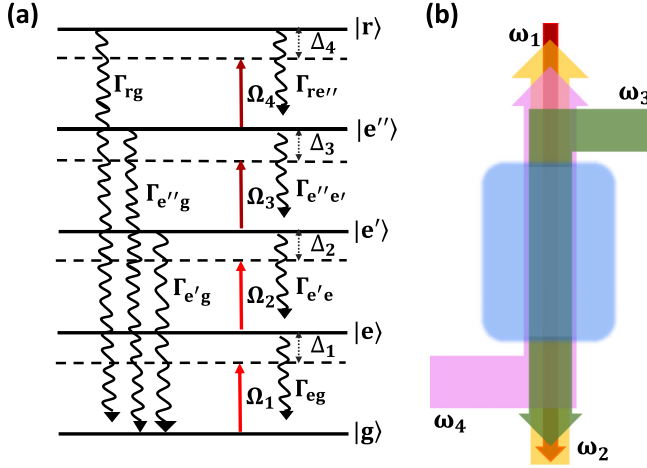
FIG. 1. (a) Schematic of the energy-level diagram of a five-level system in the ladder configuration. (b) Schematic of the laser geometry through a Rb vapor cell consisting of four laser fields of frequencies ω_1 (red), ω_2 (yellow), ω_3 (olive), and ω_4 (magenta). The laser field with frequency ω_2 (ω_4) counterpropagates the field with frequency ω_1 (ω_3), whereas ω_1 (ω_2) and ω_3 (ω_4) copropagate with each other.

and $|e\rangle$, $|e'\rangle$, and $|e''\rangle$ are the intermediate states. The four laser fields with optical frequencies ω_1, ω_2, ω_3, and ω_4 are used to carry out the dipole-allowed transitions $|g\rangle \rightarrow |e\rangle$, $|e\rangle \rightarrow |e'\rangle$, $|e'\rangle \rightarrow |e''\rangle$, and $|e''\rangle \rightarrow |r\rangle$, respectively, as shown in Fig. 1(b). The corresponding Rabi frequencies (detunings) are Ω_1 (Δ_1), Ω_2 (Δ_2), Ω_3 (Δ_3), and Ω_4 (Δ_4). The Hamiltonian of the system in a suitable rotating frame, after application of the rotating-wave approximation, can be written as

$$H = -\frac{\hbar}{2} \begin{pmatrix} 0 & \Omega_1 & 0 & 0 & 0 \\ \Omega_1^* & 2\delta_1 & \Omega_2 & 0 & 0 \\ 0 & \Omega_2^* & 2\delta_2 & \Omega_3 & 0 \\ 0 & 0 & \Omega_3^* & 2\delta_3 & \Omega_4 \\ 0 & 0 & 0 & \Omega_4^* & 2\delta_4 \end{pmatrix},$$

where $\delta_1 = \Delta_1$, $\delta_2 = (\Delta_1 + \Delta_2)$, $\delta_3 = (\Delta_1 + \Delta_2 + \Delta_3)$, and $\delta_4 = (\Delta_1 + \Delta_2 + \Delta_3 + \Delta_4)$. The optical Bloch equation for the system is given by $\dot{\rho} = \frac{i}{\hbar}[\rho, H] + \mathcal{L}_\mathcal{D}(\rho)$, where ρ is the density matrix of the system. The second term $\mathcal{L}_\mathcal{D}(\rho)$ in the equation is the Lindblad operator, which includes all the decay and decoherence processes occurring in the system and is given by $\mathcal{L}_\mathcal{D} = \sum_{if} \Gamma_{if}[C_{if}\rho C_{if}^\dagger - \frac{1}{2}\{C_{if}^\dagger C_{if}, \rho\}]$ [37]. C_{if} is defined as $C_{if} = |f\rangle\langle i|$, where $|f\rangle$ is the final state and $|i\rangle$ is the initial state. Γ_{if} represents the population decay from the initial state $|i\rangle$ to the final state $|f\rangle$. The population decay rates through the decay channels with dipole-allowed transitions, i.e., Γ_{eg}, $\Gamma_{e'e}$, $\Gamma_{e''e'}$, and $\Gamma_{re''}$ are taken to be nonzero. We also introduce the population decay of the excited states due to finite transit time of the thermal atoms through the transverse direction of the laser beams. When an atom goes out of the beam and a new atom enters the beam it remains initially in the ground state. So, the additional decay of the excited states to the ground state with respective rates Γ_{rg}, $\Gamma_{e''g}$, $\Gamma_{e'g}$, and Γ_{eg} are also taken to be nonzero. The decay rates considered in the model for the calculations are $\Gamma_{eg} = 6$ MHz, $\Gamma_{e'e} = $
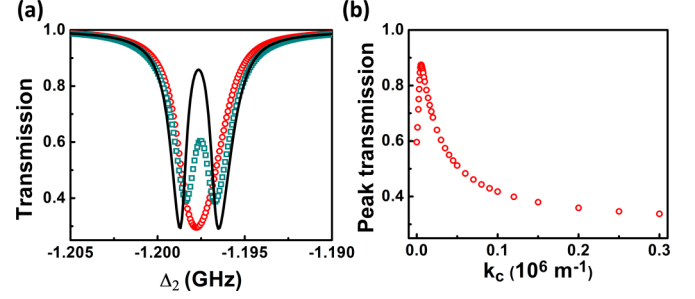
FIG. 2. (a) Probe transmission in the absence of coupling beams while scanning Δ_2 (open red circles) and in the presence of coupling beam using the five-level system with $\Delta k = 0$ (solid black line) and with $\Delta k = 0.023 \times 10^6$ m^{-1} (open green squares). The effective wave vector of the probe is used to be $k_p = 0.007 \times 10^6$ m^{-1}. (b) The probe transmission peak height as a function of k_c (open red circles). The laser parameters used in the model are $\Omega_1 = 10$ MHz, $\Omega_2 = 110$ MHz, $\Omega_3 = 80$ MHz and $\Omega_4 = 80$ MHz, $\Delta_1 = 1200$ MHz, $\Delta_3 = 1000$ MHz, and Δ_4 is adjusted around Δ_3 such that the transmission is symmetric.

0.65 MHz, $\Gamma_{e''e'} = 0.3$ MHz, $\Gamma_{re''} = 0.01$ MHz. The transit time decay rates are taken to be 0.2 MHz.

The optical Bloch equations are solved for the steady state, i.e., $\dot{\rho} = 0$, to find out the susceptibility of the probe beam. Since we are working with a thermal vapor system, by taking into consideration the velocity of the atoms in the vapor to be v and for the given laser configuration as shown in Fig. 1(b), the detunings are taken as $\Delta_1 \rightarrow \Delta_1 - k_1 v$, $\Delta_2 \rightarrow \Delta_2 + k_2 v$, $\Delta_3 \rightarrow \Delta_3 - k_3 v$, and $\Delta_4 \rightarrow \Delta_4 + k_4 v$. k_1, k_2, k_3, and k_4 are the magnitude of the wave vectors of the four driving lasers. Assuming that $k_2 > k_1$ and $k_3 > k_4$, we define $k_p = k_2 - k_1$, $k_c = k_3 - k_4$, and the residual wave vector as $\Delta k = k_c - k_p$, where $k_p(k_c)$ is termed the effective wave vector of the probe (coupling) laser beam. Doppler-averaged susceptibility of the probe beam coupling the transition $|g\rangle \rightarrow |e\rangle$ is given by $\chi(\omega_1) = \frac{2N|\mu_{ge}|^2}{\hbar\epsilon_0\Omega_1} \frac{1}{\sqrt{2\pi}v_p} \int_{-\infty}^{+\infty} \rho_{eg} e^{-v^2/2v_p^2} dv$, where μ_{ge} is the dipole moment of the $|g\rangle \rightarrow |e\rangle$ transition, N is the vapor density, and v_p is the most probable speed of the atoms. The transmission of the probe beam is calculated as $T = I/I_0 = e^{-\text{Im}(\chi)k_1 l}$, where l is the length of the vapor cell. The probe transmissions for different laser parameters are depicted in Fig. 2(a). The vapor density and length of the vapor cell are taken to be 4.5×10^{10} cm^{-3} and 5 cm, respectively. With the given laser parameters, none of the lasers satisfies the single-photon resonance, but the two-photon resonances for the transitions $|g\rangle \rightarrow |e'\rangle$ and $|e'\rangle \rightarrow |r\rangle$ are satisfied to find the EIT regime for the probe. It is to be noted that we take $k_p = 0.007 \times 10^6$ m^{-1} for the calculation. We get the peak EIT transmission to be ~ 0.9 with $\Delta k = 0$, whereas the same reduces to ~ 0.6 with $\Delta k = 0.023 \times 10^6$ m^{-1}, as depicted in Fig. 2(a). A Doppler-free condition of $\Delta k = 0$ can be achieved easily with this system leading to approximately 100% transmission of the probe, which cannot be achieved with the usual two-photon excitation [27] process with thermal vapor. As reported in [34], the three-photon excitation to the Rydberg state can also offer the Doppler-free condition for EIT with a specific beam geometry. We further study the
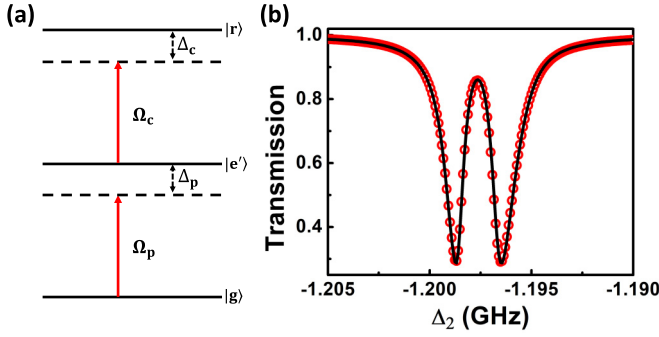
FIG. 3. (a) Schematic of the energy-level diagram of an effective three-level system in the ladder configuration. (b) Comparison of the transmission of the probe beam of a five-level system (open red circles) with an effective-three level system (solid black line) for residual wave vector $\Delta k = 0$. The laser parameters used in the model are $\Omega_1 = 10$ MHz, $\Omega_2 = 110$ MHz, $\Omega_3 = 80$ MHz and $\Omega_4 = 80$ MHz, $\Delta_1 = 1200$ MHz, $\Delta_3 = 1000$ MHz, and Δ_4 is adjusted around Δ_3 such that the transmission is symmetric.

peak EIT transmission as a function of residual wave vector by varying k_c, which is depicted in Fig. 2(b). Maximum EIT transmission is observed with $\Delta k \approx 0$, as expected. However, the transmission peak height decreases as we vary k_c away from $\Delta k = 0$. With $\Delta k = 0$, all the atoms irrespective of their velocities in a thermal vapor can be resonant to the probe and coupling lasers and hence form the dark state contributing to the maximum EIT transmission. With $\Delta k \neq 0$, a certain velocity class of atoms becomes resonant to both the probe and coupling lasers. Hence, the effective number atoms contributing to the EIT transmission reduces.

III. ADIABATIC ELIMINATION OF THE INTERMEDIATE STATES: EFFECTIVE THREE-LEVEL SYSTEM

Under the conditions of adiabatic elimination, i.e., $\Delta_1 \gg \Omega_1, \Gamma_{eg}$, and $\Delta_3 \gg \Omega_3, \Gamma_{e''e'}$ [36], the five-level system can be reduced to an effective three-level system by eliminating the intermediate states $|e\rangle$ and $|e''\rangle$. The effective three-level system is represented by states $|g\rangle$, $|e'\rangle$, and $|r\rangle$, with the effective probe (coupling) Rabi frequency and effective detuning as Ω_p (Ω_c) and Δ_p (Δ_c), respectively, as represented in Fig. 3(a). The effective Hamiltonian for the system can be written as

$$ H_{eff} = -\frac{\hbar}{2} \begin{pmatrix} 0 & \Omega_p & 0 \\ \Omega_p^* & 2\Delta_p & \Omega_c \\ 0 & \Omega_c^* & 2(\Delta_p + \Delta_c) \end{pmatrix}. $$

The Hamiltonian of the effective system is similar to that of a usual three-level system, with effective Rabi frequency and effective detuning modified as $\Omega_p = \frac{\Omega_1 \Omega_2}{2\Delta_1}$, $\Omega_c = \frac{\Omega_3 \Omega_4}{2\Delta_3}$, $\Delta_p = (\Delta_1 + \Delta_2) + \frac{|\Omega_1|^2}{4\Delta_1} - \frac{|\Omega_2|^2}{4\Delta_1} - \frac{|\Omega_3|^2}{4\Delta_3}$, and $\Delta_c = (\Delta_3 + \Delta_4) + \frac{|\Omega_2|^2}{4\Delta_1} + \frac{|\Omega_3|^2}{4\Delta_3} - \frac{|\Omega_4|^2}{4\Delta_3}$. It is to be noted that the relevant light shift factors are included to the laser detunings appropriately to get the effective detunings for the three-level system. The density matrix ρ of the effective three-level system is given by a 3×3 matrix. We assume that the decay rate from state $|e\rangle$ to state $|g\rangle$ is much faster than the decay rate from state $|e'\rangle$

to state $|e\rangle$, i.e., $\Gamma_{eg} \gg \Gamma_{e'e}$. So, there won't be any population inversion in $|e\rangle$, and the atoms in the state $|e'\rangle$ can be considered to decay directly to state $|g\rangle$ at a rate of $\Gamma_{e'e}$. Similarly, we can assume that $\Gamma_{e''e'} \gg \Gamma_{re''}$, and the atoms in state $|r\rangle$ can be considered to decay to state $|e'\rangle$ at a rate of $\Gamma_{re''}$. Now, including the population decay due to the finite transit time of atoms through the transverse direction of the beams, the effective decay rates of the channels $|r\rangle \rightarrow |e'\rangle$, $|r\rangle \rightarrow |g\rangle$, and $|e'\rangle \rightarrow |g\rangle$ are $\gamma_{re'} \approx \Gamma_{re''}$, $\gamma_{rg} = \Gamma_{rg}$, and $\gamma_{e'g} \approx \Gamma_{e'e} + \Gamma_{e'g}$, respectively. The Lindblad operator for the effective system is written by considering these effective decay rates. The optical Bloch equations for the effective system are solved in steady state, i.e., $\dot{\rho} = 0$, to evaluate $\rho_{e'e'}$ and $\rho_{e'g}$. ρ_{eg} is expressed in terms of $\rho_{e'g}$ and $\rho_{e'e'}$ as [27]

$$ \rho_{eg} = \frac{\Omega_1(\rho_{e'e'} - 1) - \Omega_2 \rho_{e'g}}{2\Delta_1 + i\Gamma_{eg}}. \tag{1} $$

Doppler-averaged susceptibility of the probe beam is further calculated using the same method as discussed in Sec. II. The comparison between the calculated probe transmission using the effective three-level system and the exact five-level system is illustrated in Fig. 3(b). The excellent match between both the methods suggests that by using the method of adiabatic elimination with suitable approximation for a wide range of laser parameters, the complex five-level system can be reduced to an effective three-level system to study the many-body interactions in the Rydberg state.

IV. INTERACTING TWO-ATOM SYSTEM

In order to study the effect of Rydberg-Rydberg interactions, we consider the case of a two-atom system with the energy-level diagram illustrated in Fig. 4. Each atom is considered to be in an effective three-level system consisting of states $|g\rangle$, $|e'\rangle$, and $|r\rangle$. The energy levels of the composite system $|1\rangle$, $|4\rangle$, and $|9\rangle$ are considered when both the atoms are in states $|g\rangle$, $|e'\rangle$, and $|r\rangle$, respectively. The energy levels $|2\rangle$ and $|3\rangle$ are considered when one atom is in state $|g\rangle$ and the other atom is in state $|e'\rangle$ and vice versa. Similarly, energy levels $|5\rangle$ and $|6\rangle$ ($|7\rangle$ and $|8\rangle$) are considered when one atom is in state $|g\rangle$ ($|e\rangle$) and the other atom is in state $|r\rangle$ and vice versa. Both the atoms in the thermal vapor are considered to move with independent velocities v_1 and v_2. Hence, the probe (coupling) detunings for both atoms are taken to be independent as Δ_{p_1} (Δ_{c_1}) and Δ_{p_2} (Δ_{c_2}). Similarly, the probe (coupling) Rabi frequencies for both atoms are taken to be Ω_{p_1} (Ω_{c_1}) and Ω_{p_2} (Ω_{c_2}). Strong van der Waals interaction between the atoms in the Rydberg state shift the energy level $|9\rangle$ by Δ_{int}. Since we consider the van der Waals interaction to be repulsive, Δ_{int} is taken to be positive. The interacting Hamiltonian for the composite system is written as $H = H^{(1)} \otimes I + I \otimes H^{(2)} + \Delta_{int}|9\rangle\langle9|$, where $H^{(1)}$, $H^{(2)}$ are the Hamiltonian of the individual atoms and I is the identity matrix. The Lindblad operator of the composite system is taken as $\mathcal{L}_D(\rho) = \mathcal{L}_{D_1}(\rho^{(1)}) \otimes \rho^{(2)} + \rho^{(1)} \otimes \mathcal{L}_{D_2}(\rho^{(2)})$, where $\mathcal{L}_{D_1}(\rho^{(1)})$, $\mathcal{L}_{D_2}(\rho^{(2)})$ are the individual Lindblad operators for the individual atoms, with $\rho^{(1)}$ and $\rho^{(2)}$ being the individual density matrices.

We solve the optical Bloch equations for the composite system to determine $\rho_{e'e'}$ and $\rho_{e'g}$, which are given
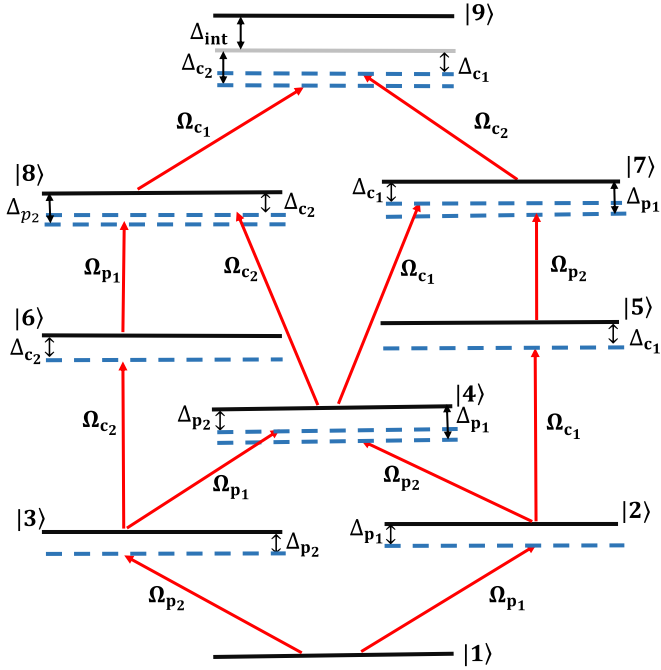
FIG. 4. Schematic of the energy-level diagram of the composite two-atom system where the individual atoms are considered to be in the effective three-level system in the ladder configuration.

as $\rho_{e'e'} = \rho_{44} + \frac{1}{2}(\rho_{22} + \rho_{33} + \rho_{77} + \rho_{88})$ and $\rho_{e'g} = \frac{1}{2}(\rho_{21} + \rho_{31} + \rho_{42} + \rho_{43} + \rho_{75} + \rho_{86})$. Here we consider $\Omega_{p1} = \Omega_{p2}$, and without loss of generality, Rabi frequencies are chosen to be real. The ground intermediate state coherence ρ_{eg} is calculated using Eq. (1) by substituting the expressions for $\rho_{e'e'}$ and $\rho_{e'g}$ as discussed in Sec. III. We consider both atoms to move with independent velocities and Doppler-averaged susceptibility is calculated as

$$\chi = \frac{2N|\mu_{ge}|^2}{\hbar\epsilon_0\Omega_1} \frac{1}{\pi v_p{}^2} \int_{-\infty}^{+\infty} \int_{-\infty}^{+\infty} \rho_{eg} e^{\frac{-(v_1^2+v_2^2)}{v_p^2}} \, dv_1 dv_2. \quad (2)$$

This integral is solved using the Monte Carlo simulation technique. The probe transmission is calculated for different

experimental parameters and presented in Fig. 5. Absence of the residual wave vector ($\Delta k = 0$) leads the EIT transmission to be close to 90% for the noninteracting case, whereas the blockade effect due to strong Rydberg-Rydberg interaction suppresses the EIT transmission as shown in Fig. 5(a). The absence of motion-induced dephasing in this case makes the blockade effect similar to the observations in ultracold atoms [38]. If a small residual wave vector is introduced in the system, i.e., $\Delta k = 0.013 \times 10^6$ m^{-1}, then we observe that the EIT transmission is reduced for the noninteracting case, as explained in Sec. II, and the blockade-induced suppression for the case of strong Rydberg-Rydberg interaction is also reduced, as illustrated in Fig. 5(b). We define the normalized blockaded transmission as the ratio of blockaded probe transmission to the probe transmission for the noninteracting case. We further investigate the normalized blockaded transmission as a function of k_c, which is shown in Fig. 5(c). With increase in k_c, a reduced blockade effect is observed, which can be understood as the reduced effective number of atoms participating in the blockade process due to the increase in residual wave vector, allowing a certain velocity class of atoms resonating in the EIT process. The other dephasing mechanism in the thermal vapor system which can occur due to the transverse velocity of the atoms can also be investigated. If an atom moves out of the blockade sphere and another atom enters, then there will be a dephasing introduced in the multiatom coherence due to the Rydberg blockade. This is called the superatom dephasing (Γ_S) and is discussed in detail in Ref. [39]. Superatom dephasing can be introduced in the calculation as the dephasing of the coherence between the singly excited Rydberg states. So, Γ_S can be included in the $\mathcal{L}_D$ matrix as the dephasing of ρ_{56} and ρ_{78} of the composite system. It is worth noting that if $2r_b\Delta k > 1$, where r_b is the blockade radius, then Γ_S can be calculated using the transit time of the atoms through the blockade sphere. However, if $2r_b\Delta k < 1$, then the superatom dephasing in the system is $\Delta k v_{avg}$, where v_{avg} is the average velocity of the atoms [39]. If $\Delta k \sim 0$, then the transit time of the atoms through the beam dominates the decoherence in the system, which can be of the order of 100 KHz by using a beam size of 1 mm.
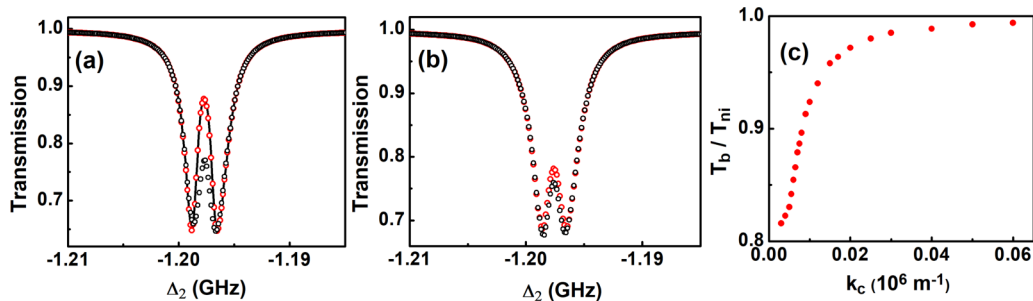
FIG. 5. (a) Comparison of the probe transmission calculated using a single-atom system (solid black line), noninteracting two-atom system (open red circles), and interacting two-atom system with $\Delta_{int} = 100$ MHz (open black circles). The residual wave vector used in the calculation as $\Delta k = 0$. (b) Comparison of the probe transmission calculated using noninteracting two-atom system (open red circles) and interacting two-atom system with $\Delta_{int} = 100$ MHz (open black circles). The residual wave vector used in the calculation as $\Delta k = 0.013 \times 10^6$ m^{-1}. (c) Normalized blockaded transmission as a function of k_c with $k_p = 0.007 \times 10^6$ m^{-1} for $\Delta_{int} = 100$ MHz. The laser parameters used in the model are $\Omega_1 = 40$ MHz, $\Omega_2 = 120$ MHz, $\Omega_3 = 90$ MHz and $\Omega_4 = 90$ MHz, $\Delta_1 = 1200$ MHz, $\Delta_3 = 1000$ MHz, and Δ_4 is adjusted around Δ_3 such that the transmission is symmetric.
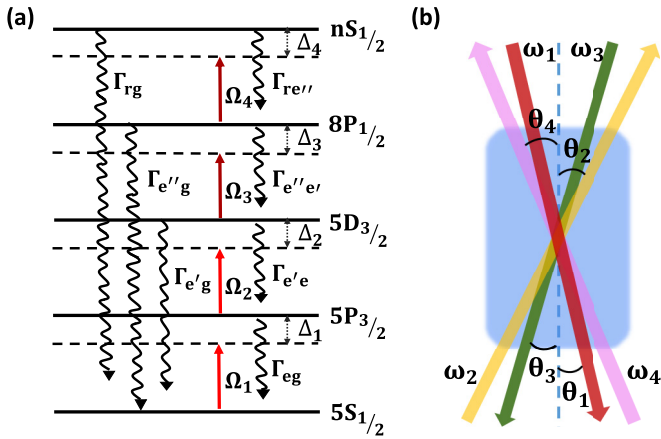
FIG. 6. (a) Energy-level diagram of a five-level system in the ladder configuration for rubidium vapor. (b) Schematic of the laser geometry through a rubidium vapor cell. The lasers with frequencies ω_1, ω_2, ω_3, and ω_4 propagate through the vapor cell with angles θ_1, θ_2, θ_3, and θ_4, respectively.

It is worth mentioning that if $\Delta_{\text{int}} \gg \gamma_{EIT}$ where γ_{EIT} is the EIT linewidth, the blockade effect does not depend on the interaction shift of the Rydberg state [38]. This is also verified with our code for the proposed system. For the sake of analysis, we consider $\Delta_{\text{int}} = 100\,\text{MHz}$, which is much greater than the typical EIT linewidth of $2\,\text{MHz}$ for the system. To explore a typical experimental situation, the number of atoms in the blockade sphere is given by $N_b = N\frac{4}{3}\pi r_b^3$, where the blockade radius is defined as $r_b = \sqrt[6]{\frac{C_6}{\gamma_{EIT}}}$ [38]. Here, C_6 is the coefficient of the van der Waals interaction. If the lasers are tuned to excite to the $35S_{\frac{1}{2}}$ state for the vapor density used for the simulation, then on an average there are two atoms in the blockade sphere. However, the number of atoms in the blockade sphere can be varied with vapor density or by driving the system to a Rydberg state with different principal quantum number. If there are n atoms in a blockade sphere, then we need a model with n interacting atoms to study the blockade effect in the system. All the atoms in the blockade sphere are collectively excited and behave like a single superatom. The absorption of the probe laser beam is then given by an ensemble average of all the superatoms present in the interaction volume of the laser beam interacting with the atomic vapor [39]. It is to be noted that the simple two-atom model presented here cannot be directly applied to analyze the results obtained for blockade phenomenon in a typical experiment. It is just a proof of principle to observe the blockade phenomenon in the thermal vapor system.

V. EXPERIMENTAL PROPOSAL

We present a proposal for the experimental study of four-photon excitation in a real thermal vapor system, i.e., rubidium vapor system. As can be seen from Fig. 6(a),

the four-photon excitation can be carried out in a five-level system consisting of the different allowed transitions of rubidium. The transitions $|5S_{\frac{1}{2}}\rangle \rightarrow |5P_{\frac{3}{2}}\rangle$, $|5P_{\frac{3}{2}}\rangle \rightarrow |5D_{\frac{3}{2}}\rangle$, $|5D_{\frac{3}{2}}\rangle \rightarrow |8P_{\frac{1}{2}}\rangle$, and $|8P_{\frac{1}{2}}\rangle \rightarrow |nS_{\frac{1}{2}}\rangle$ are carried out by using lasers of wavelength 780.24 nm, 776.2 nm, 2.41 μm, and 2.67 μm, respectively. Their corresponding wave vectors are $k_1 = 1.281\,655 \times 10^6$ m^{-1}, $k_2 = 1.288\,328 \times 10^6$ m^{-1}, $k_3 = 0.414\,938 \times 10^6$ m^{-1}, and $k_4 = 0.374\,532 \times 10^6$ m^{-1}, respectively. The transitions $|5S_{\frac{1}{2}}\rangle \rightarrow |5D_{\frac{3}{2}}\rangle$, $|5P_{\frac{3}{2}}\rangle \rightarrow |8P_{\frac{1}{2}}\rangle$, and $|5D_{\frac{3}{2}}\rangle \rightarrow |nS_{\frac{1}{2}}\rangle$ are dipole forbidden. The decay rates for the rubidium system are $\Gamma_{eg} = 6\,\text{MHz}$, $\Gamma_{e'e} = 0.65\,\text{MHz}$, $\Gamma_{e''e'} = 0.3\,\text{MHz}$, $\Gamma_{re''} = 0.01\,\text{MHz}$. The transit time decay rates Γ_{rg}, $\Gamma_{e''g}$, $\Gamma_{e'g}$ are taken to be 0.2 MHz. If we take into consideration the laser configuration shown in Fig. 1(b), $k_p = k_2 - k_1$ and $k_c = k_3 - k_4$. The residual wave vector is calculated as $\Delta k = 0.033 \times 10^6$ m^{-1}. With such a large residual wave vector, we observe a very low transparency for EIT, as shown in Fig. 2(b), and also the blockade effect is inefficient at this regime. However, as shown in Fig. 6(b), by introducing suitable angles between the lasers, Δk can be changed within the range to observe efficient EIT as well as the Rydberg blockade. In order to completely cancel out the wave-vector mismatch, i.e., to make $\Delta k \sim 0$, the angles are calculated to be $\theta_1 = 6°$, $\theta_2 = 6°$, $\theta_3 = 3°$, and $\theta_4 = 3°$ with respect to the axis of the cylindrical vapor cell. Since the angles are small, then the overlapping of the beams over a large optical path length can be maintained, which would be advantageous over the ultracold atoms.

VI. CONCLUSION

We present a model for the four-photon excitation process to the Rydberg state in thermal atomic vapor and discuss the role of the wave-vector mismatch on the probe transmission in the EIT regime. We demonstrate that even though it is a thermal vapor system, by reducing the residual wave vector to zero using suitable laser geometry, the motion-induced dephasing can be eliminated. Using this model, EIT is studied in the strong blockade regime by taking into consideration a two-atom interacting system. The blockade phenomenon observed is similar to a cold atomic system for the case where the residual wave vector is zero. So, instead of going for a complex cold atom system, quantum many-body systems can be studied in this simpler thermal vapor system using strong optical nonlinearity induced by the Rydberg blockade phenomenon. This will pave the way for applications in the field of quantum technology as Rydberg atoms play an important role in building quantum devices.

[1] T. F. Gallagher, Rydberg atoms, Rep. Prog. Phys. **51**, 143 (1988).

[2] A. Browaeys and T. Lahaye, Many-body physics with individually controlled Rydberg atoms, Nat. Phys. **16**, 132 (2020).

[3] F. Carollo, F. M. Gambetta, K. Brandner, J. P. Garrahan, and I. Lesanovsky, Nonequilibrium Quantum Many-Body Rydberg Atom Engine, Phys. Rev. Lett. **124**, 170602 (2020).

[4] T. Peyronel, O. Firstenberg, Q.-Y. Liang, S. Hofferberth, A. V. Gorshkov, T. Pohl, M. D. Lukin, and V. Vuletic, Quantum non-linear optics with single photons enabled by strongly interacting atoms, Nature (London) **488**, 57 (2012).

[5] A. K. Mohapatra, M. G. Bason, B. Butscher, K. J. Weatherill, and C. S. Adams, A giant electro-optic effect using polarizable dark states, Nat. Phys. **4**, 890 (2008).

[6] S. Kumar, H. Fan, H. Kübler, J. Sheng, and J. P. Shaffer, Atom-based sensing of weak radio frequency electric fields using homodyne readout, Sci. Rep. **7**, 42981 (2017).

[7] J. A. Sedlacek, A. Schwettmann, H. Kübler, R. Löw, T. Pfau, and J. P. Shaffer, Microwave electrometry with Rydberg atoms in a vapour cell using bright atomic resonances, Nat. Phys. **8**, 819 (2012).

[8] C. G. Wade, N. Šibalić, N. R. de Melo, J. M. Kondo, C. S. Adams, and K. J. Weatherill, Real-time near-field terahertz imaging with atomic optical fluorescence, Nat. Photonics **11**, 40 (2017).

[9] T. Baluktsian, B. Huber, R. Löw, and T. Pfau, Evidence for Strong van der Waals Type Rydberg-Rydberg Interaction in a Thermal Vapor, Phys. Rev. Lett. **110**, 123001 (2013).

[10] M. Saffman, T. G. Walker, and K. Mølmer, Quantum information with Rydberg atoms, Rev. Mod. Phys. **82**, 2313 (2010).

[11] M. Fleischhauer, A. Imamoglu, and J. P. Marangos, Electro-magnetically induced transparency: Optics in coherent media, Rev. Mod. Phys. **77**, 633 (2005).

[12] A. K. Mohapatra, T. R. Jackson, and C. S. Adams, Coherent Optical Detection of Highly Excited Rydberg States Using Electromagnetically Induced Transparency, Phys. Rev. Lett. **98**, 113003 (2007).

[13] D. Petrosyan, J. Otterbach, and M. Fleischhauer, Electromagnetically Induced Transparency with Rydberg Atoms, Phys. Rev. Lett. **107**, 213601 (2011).

[14] A. V. Gorshkov, J. Otterbach, M. Fleischhauer, T. Pohl, and M. D. Lukin, Photon-Photon Interactions Via Rydberg Blockade, Phys. Rev. Lett. **107**, 133602 (2011).

[15] S. Sevinçli, N. Henkel, C. Ates, and T. Pohl, Nonlocal Nonlinear Optics in Cold Rydberg Gases, Phys. Rev. Lett. **107**, 153001 (2011).

[16] O. Firstenberg, T. Peyronel, Q.-Y. Liang, A. V. Gorshkov, M. D. Lukin, and V. Vuletic, Attractive photons in a quantum nonlinear medium, Nature (London) **502**, 71 (2013).

[17] M. Saffman and T. G. Walker, Creating single-atom and single-photon sources from entangled atomic ensembles, Phys. Rev. A **66**, 065403 (2002).

[18] O. Firstenberg, C. S. Adams, and S. Hofferberth, Nonlinear quantum optics mediated by Rydberg interactions, J. Phys. B: At., Mol. Opt. Phys. **49**, 152003 (2016).

[19] H. Busche, P. Huillery, S. W. Ball, T. Ilieva, M. P. A. Jones, and C. S. Adams, Contactless nonlinear optics mediated by long-range Rydberg interactions, Nat. Phys. **13**, 655 (2017).

[20] M. D. Lukin, M. Fleischhauer, R. Cote, L. M. Duan, D. Jaksch, J. I. Cirac, and P. Zoller, Dipole Blockade and Quantum Information Processing in Mesoscopic Atomic Ensembles, Phys. Rev. Lett. **87**, 037901 (2001).

[21] E. Urban, T. A. Johnson, T. Henage, L. Isenhower, D. D. Yavuz, T. G. Walker, and M. Saffman, Observation of Rydberg block-ade between two atoms, Nat. Phys. **5**, 110 (2009).

[22] A. Gaëtan, Y. Miroshnychenko, T. Wilk, A. Chotia, M. Viteau, D. Comparat, P. Pillet, A. Browaeys, and P. Grangier, Observation of collective excitation of two individual atoms in the Rydberg blockade regime, Nat. Phys. **5**, 115 (2009).

[23] D. Tong, S. M. Farooqi, J. Stanojevic, S. Krishnan, Y. P. Zhang, R. Côté, E. E. Eyler, and P. L. Gould, Local Blockade of Rydberg Excitation in an Ultracold Gas, Phys. Rev. Lett. **93**, 063001 (2004).

[24] K. Singer, M. Reetz-Lamour, T. Amthor, L. G. Marcassa, and M. Weidemüller, Suppression of Excitation and Spectral Broadening Induced by Interactions in a Cold Gas of Rydberg Atoms, Phys. Rev. Lett. **93**, 163001 (2004).

[25] A. Bhowmick, D. Kara, and A. K. Mohapatra, Study of Rydberg blockade in thermal vapor, arXiv:1802.06599.

[26] F. Ripka, H. Kübler, R. Löw, and T. Pfau, A room-temperature single-photon source based on strongly interacting Rydberg atoms, Science **362**, 446 (2018).

[27] A. Bhowmick, D. Kara, and A. K. Mohapatra, High-sensitivity measurement of Rydberg population via two-photon excitation in atomic vapour using optical heterodyne detection technique, Pramana **92**, 76 (2019).

[28] D. Kara, A. Bhowmick, and A. K. Mohapatra, Rydberg interaction induced enhanced excitation in thermal atomic vapor, Sci. Rep. **8**, 5256 (2018).

[29] C. Carr, R. Ritter, C. G. Wade, C. S. Adams, and K. J. Weatherill, Nonequilibrium Phase Transition in a Dilute Rydberg Ensemble, Phys. Rev. Lett. **111**, 113901 (2013).

[30] C. Carr, M. Tanasittikosol, A. Sargsyan, D. Sarkisyan, C. S. Adams, and K. J. Weatherill, Three-photon electromagnetically induced transparency using Rydberg states, Opt. Lett. **37**, 3858 (2012).

[31] J. M. Kondo, N. Šibalić, A. Guttridge, C. G. Wade, N. R. D. Melo, C. S. Adams, and K. J. Weatherill, Observation of interference effects via four-photon excitation of highly excited Rydberg states in thermal cesium vapor, Opt. Lett. **40**, 5570 (2015).

[32] F. Bariani, Y. O. Dudin, T. A. B. Kennedy, and A. Kuzmich, Dephasing of Multiparticle Rydberg Excitations for Fast Entanglement Generation, Phys. Rev. Lett. **108**, 030501 (2012).

[33] R. Finkelstein, O. Lahad, I. Cohen, O. Davidson, S. Kiriati, E. Poem, and O. Firstenberg, Continuous Protection of a Collective State from Inhomogeneous Dephasing, Phys. Rev. X **11**, 011008 (2021).

[34] N. Šibalić, J. M. Kondo, C. S. Adams, and K. J. Weatherill, Dressed-state electromagnetically induced transparency for light storage in uniform-phase spin waves, Phys. Rev. A **94**, 033840 (2016).

[35] C. S. Adams, J. D. Pritchard, and J. P. Shaffer, Rydberg atom quantum technologies, J. Phys. B: At. Mol. Opt. Phys. **53**, 012002 (2019).

[36] R. Han, H. K. Ng, and B.-G. Englert, Raman transitions without adiabatic elimination: A simple and accurate treatment, J. Mod. Opt. **60**, 255 (2013).

[37] G. Lindblad, On the generators of quantum dynamical semigroups, Commun. Math. Phys. **48**, 119 (1976).

[38] J. D. Pritchard, D. Maxwell, A. Gauguet, K. J. Weatherill, M. P. A. Jones, and C. S. Adams, Cooperative Atom-Light Interaction in a Blockaded Rydberg Ensemble, Phys. Rev. Lett. **105**, 193603 (2010).

[39] D. Kara and A. K. Mohapatra, Study of the effect of super-atom dephasing on Rydberg blockade in thermal vapor, J. Phys. B: At. Mol. Opt. Phys. **53**, 245301 (2020).